Sequential Two-Photon Dissociation of Atmospheric Water

Lisa M. Goss, Veronica Vaida, James W. Brault, and Rex T. Skodje*

Department of Chemistry and Biochemistry, University of Colorado, Boulder Colorado 80309

Received: May 18, 2000; In Final Form: August 30, 2000

A new mechanism is proposed for the atmospheric production of OH radicals. The mechanism involves a sequential two-photon absorption by atmospheric H_2O molecules. The first photon excites H_2O to a high vibrational state (H_2O^*), and the second promotes H_2O^* to a dissociative electronic state. Theoretical calculations are combined with the results of experimental measurement to assess the importance of this mechanism as a source of atmospheric OH. The collisional quenching rate of H_2O^* is found to be a crucial factor in the relative contribution of the proposed mechanism to OH production at different altitudes. We believe that it is likely that the quenching rate is too rapid for the two-photon mechanism to contribute significantly in the atmosphere, although the energy transfer rates for highly excited H_2O^* have yet to be measured in the laboratory.

I. Introduction

The chemistry of the hydroxyl radical, OH, provides the most important means by which oxidation processes are initiated in the chemistry of the Earth's atmosphere.[1−4] At high altitudes, particularly above 45 km, OH participates in catalytic O_3 loss. Water in the atmosphere plays an important chemical role in the formation of OH. The main source of odd hydrogen ($HO_x = OH + HO_2 + H$) in the stratosphere is, according to conventional models, the reaction of excited oxygen atoms with water vapor. $O(^1D)$ is produced with a high quantum yield by the photodissociation of ozone at wavelengths less than 310 nm and by a low-efficiency process at higher wavelengths.[5] However, the contribution to OH production from direct photolysis of H_2O is limited by the spectrum of light available in the atmosphere and is not believed to be important except in the upper mesosphere and the thermosphere.[6] The first excited electronic state of H_2O is a purely repulsive (i.e., dissociative) state of $^1A_1$ symmetry that we shall refer to subsequently as the $^1A_1$ state. Absorption to this state occurs at wavelengths shorter than 190 nm and leads to direct dissociation to the products H and OH.[7] Since appreciable solar intensity at these wavelengths is only available at very high altitudes (greater than 60 km), one photon dissociation of water does not contribute significantly to either stratospheric or tropospheric OH formation.

According to most atmospheric models, the main pathway for the formation of HO_x (which denotes any of the species OH, HO_2, and H) in the atmosphere is through the sequence of reactions[8,9]

$$O_3 + h\nu(\lambda < 310\ \text{nm}) \rightarrow O_2 + O(^1D) \quad (1)$$

$$O(^1D) + M \rightarrow O(^3P) + M \quad (2)$$

$$O(^1D) + H_2O \rightarrow 2OH \quad (3)$$

$$O(^1D) + CH_4 \rightarrow OH + CH_3 \quad (4)$$

The atmospheric production rate of OH via these reactions is limited in several ways. First, the concentration of O_3 in the troposphere is low, about 25 ppb. Second, the presence of O_3 higher in the stratosphere limits the intensity of solar radiation for the photolysis reaction, eq 1, by filtering out short-wavelength radiation. Finally, atmospheric N_2 and O_2 efficiently quench $O(^1D)$ to the relatively unreactive species $O(^3P)$.

The filtering effect of O_3 implies that the light intensity available at altitudes in and below the O_3 layer has sharp cutoffs near the edges of the O_3 absorption at 230 and 280 nm. As shown in Figure 1,[7] the dropoff in solar intensity is quite dramatic at altitudes below 50 km. When the sun is low in the sky at high zenith angle, the path through the atmosphere is much longer, and short wavelengths are even more strongly attenuated. Consequently, photochemical processes at lower altitudes are primarily driven by the remaining light with near-UV and visible wavelengths.

Other photolytic sources of OH radicals of some significance recently proposed[10] are the photolysis of weakly bound species such as HONO and HOBr and the solar pumping of vibrational overtones of HNO_3, HNO_4, H_2O_2,[11] and molecular complexes such as $O_3(H_2O)$.[12] These processes have been shown to occur at wavelengths longer than those of the usual process given by eqs 1−4 and have been examined as a source of observed OH at high solar zenith angles. The primary loss pathways for OH are reactions with CH_4 and CO, which are present in higher concentrations than other species that react with OH.

A central motivation of the present work is an apparent inadequacy of the ozone photolysis mechanism, eqs 1−4, to account for the observed abundance of OH radicals in the atmosphere. Observations of OH and HO_2 in the upper stratosphere[13] that have employed different techniques lead to conflicting conclusions about the concentration of these species, in particular OH. In the lower stratosphere, OH and HO_2 levels have been measured directly from high-altitude aircrafts,[14,15] yielding higher concentrations of OH than those predicted from atmospheric models.[10,15] In the lower free troposphere, measurements performed above clouds yielded large [OH]'s compared with values obtained in cloud free regions.[16] Model calculations underestimate [OH] above clouds and overestimate [OH] in the interior of clouds.[16,17] The 1993 tropospheric OH photochemical experiment in the Rocky Mountains of Colorado provided a

10.1021/jp001828a CCC: $20.00 © 2001 American Chemical Society
Published on Web 12/15/2000

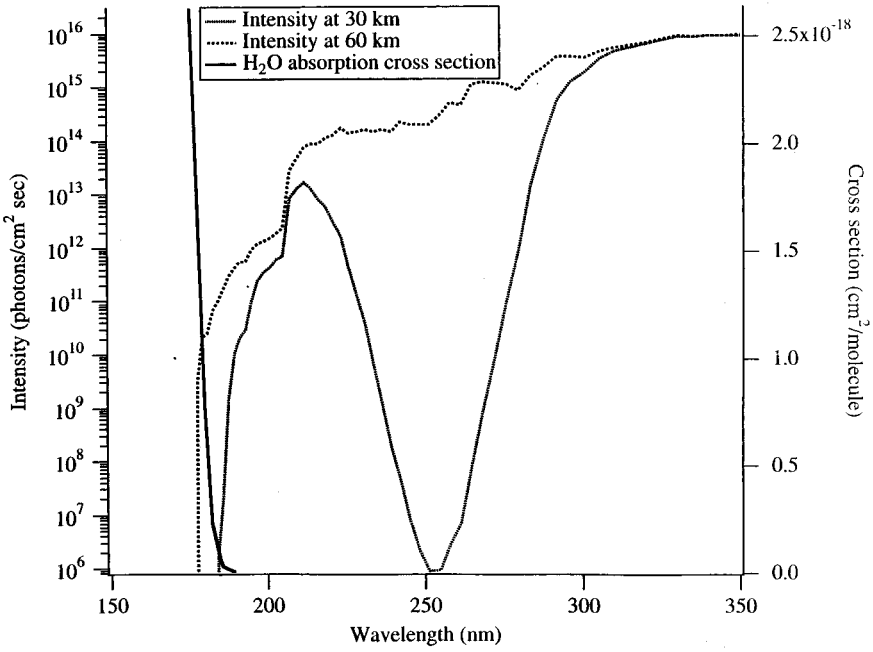

Figure 1. Intensity spectrum of solar radiation on a logarithmic scale at various altitudes in the atmosphere. At altitudes below about 50 km, the spectrum shows a sharp cutoff near 300 nm. Also plotted, but on a linear scale, is the edge of the absorption spectrum to the directly dissociative $^1A_1$ state.

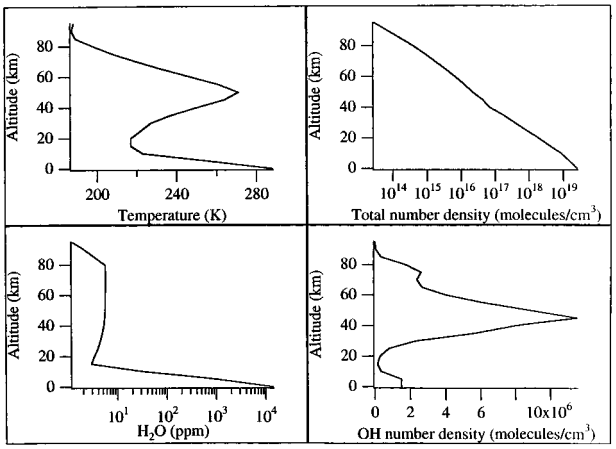

Figure 2. Altitude dependence of the important model parameters. In the first panel, the average atmospheric temperature in K is plotted vs altitude above sea level. In the second panel, the total number density of molecules is shown. In the third panel, the concentration of H_2O molecules is plotted. In the last panel, the concentration of OH radicals predicted by the standard model, eqs 1−4, is plotted.

remarkably complete data set for the study of OH and related compounds[18] as well as for other aspects of tropospheric photochemistry. A modeling study of measurements at Canary Island has also examined OH concentrations.[19] The SPADE campaign in 1993 made the first simultaneous measurements of OH and HO_2 with NO_x and ClO_x in the lower stratosphere.[15] The key point is that atmospheric models, which rely on the ozone photolysis mechanism, predict significantly lower OH concentrations than are observed. (The altitude dependence of OH concentration predicted by the model and several other important quantities are displayed in Figure 2.) Therefore, we are led to consider other mechanisms for the generation of atmospheric OH. Of interest here are the possible contributions of nonlinear photochemical effects involving solar radiation. The nonlinear process to be considered is the sequential two-photon dissociation of H_2O in the atmosphere as a result of solar pumping.

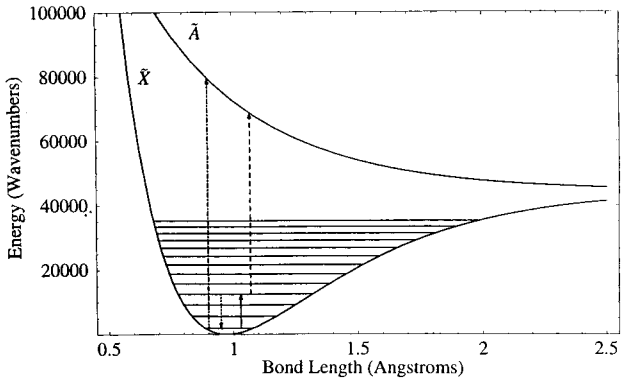

Figure 3. Two-photon photolysis mechanism. The first photon pumps ground-state water to a vibrationally excited state with a rate constant given by j_1. The second photon promotes H_2O^* to the dissociative $^1A_1$ state at rate j_2. The collisional quenching of H_2O^* is governed by the rate constant k_q.

II. Proposed Mechanism

The mechanism we propose involves solar radiation in a sequential two-photon process, which results in the photodissociation of water to produce OH radicals. The first photon creates a vibrationally excited intermediate state, while the second photon takes the system to a repulsive (i.e., dissociative) excited state. This process is illustrated in Figure 3. The first absorption is assumed to occur from the lowest vibrational state of the ground electronic state of H_2O, which we label $\tilde{X}$, to a vibrational overtone of the $\tilde{X}$ state. The second photon induces a transition to the first excited electronic state $^1A_1$, which directly dissociates to form OH and H. This mechanism is summarized by the following three-step process:

$$H_2O(\tilde{X},\mathbf{v}=0) + h\nu \xrightarrow{j_1} H_2O(\tilde{X},\mathbf{v}>0) \qquad (5)$$

$$H_2O(\tilde{X},\mathbf{v}>0) + M \xrightarrow{k_q} H_2O(\tilde{X},\mathbf{v}=0) + M \qquad (6)$$

$$H_2O(X,\mathbf{v}>0) + h\nu \xrightarrow{j_2} H_2O(\tilde{A}) \rightarrow H + OH \qquad (7)$$

The vibrational states of water are labeled by three quantum numbers. At low excitation, these quantum numbers denote the normal modes, symmetric stretch, asymmetric stretch, and bend, $\nu = (\nu_{ss},\nu_b,\nu_{as})$. At higher excitation, a local mode description is more appropriate, i.e., $(\nu_{OH_1},\nu_{OH_2},\nu_b)$. For convenience, we shall refer to any vibrationally excited water molecule on the ground surface as H_2O^*. For a completely harmonic potential, the dipole selection rule $\Delta\nu = 1$ must hold for vibrational transitions. However, when anharmonicity is included, direct overtone excitation is possible. Indeed, through its excitation to vibrational overtones in the near-IR and visible portions of the spectrum, water is found to be the most significant greenhouse gas in the Earth's atmosphere.[20] For absorption by H_2O, the overtone intensity is found to drop roughly by about a factor of 8.8 for each vibrational overtone compared with the preceding one.[21] Excitation can occur to combination states as well as to pure overtone states. We shall not require an explicit representation of the rotational quantum states.

In competition with the vibrational pumping process is the collisional quenching of H_2O^* back to the ground vibrational state. This process is crucial in determining the available population of H_2O^* for the second photon absorption. The collider, M, will be atmospheric gases O_2 and N_2 and, to a much smaller degree, other water molecules. Quenching of H_2O^* by H_2O is expected to be very efficient[22] but only quantitatively relevant at ground level. The water vapor concentration decreases rapidly with increasing altitude (see Figure 2); consequently, the dominant quenching process in the atmosphere is through the most abundant colliders, O_2 and N_2. In principle, the entire manifold of state-to-state transitions, $\mathbf{v} \rightarrow \mathbf{v}'$, must be modeled to represent the quenching kinetics. However, as we shall show in the next section, a simpler scheme can be employed.

The final step in the proposed mechanism is absorption of a solar photon by H_2O^* to the $^1A_1$ surface, which leads to direct dissociation and OH production. In the context of this two-photon mechanism, since the water molecule is already highly excited, a second photon of sufficient energy for dissociation will be abundantly available in the solar spectrum. Thus, the nonlinear process proposed effectively circumvents the solar cutoff and makes H_2O photodissociation a viable mechanism for atmospheric OH production.

III. Kinetic Analysis

To judge whether the proposed mechanism is significant for OH production in the atmosphere, we need to model the kinetics of the process in eqs 5−7. Unfortunately, a model which lumps all the excited vibrational states of water into a single species, H_2O^*, such as a Lindemann type model, is inadequate for the present problem. Since the rate of overtone pumping process (photon one) and the photodissociation rate (photon two) are highly dependent on the vibrational energy, and since the vibrational relaxation process is known to be a ladder-climbing-type process, the vibrational manifold must be retained. Thus, at first sight, the kinetic model required appears to be quite large since the populations of all the vibrationally excited states, $H_2O(\tilde{X},\mathbf{v})$, are needed. However a physically reasonable approximation, sufficient for our estimates, is to label the excited states by a single variable, the internal energy, E

$$E = E(\mathbf{v},J) - E(0) \tag{8}$$

which includes both vibrational and rotational excitation. The use of a single internal variable is justified if the internal energy is collisionally randomized very quickly. Since we shall see that many collisions generally occur before the photolysis of an excited molecule, this assumption appears reasonable. The concentrations of excited H_2O can then be represented by the function $[H_2O(E)]$. In terms of this quantity, the kinetics equations describing the photolysis process can be written as

$$\frac{d[H_2O(E)]}{dt} = j_1(E)[H_2O(0)] - [M]\int (k_q(E \rightarrow E')[H_2O(E)] - k_q(E' \rightarrow E)[H_2O(E')])\, dE' - j_2(E)[H_2O(E)] \tag{9}$$

$$\frac{d[HO_x]}{dt} = 2\int j_2(E)[H_2O(E)]\, dE \tag{10}$$

The concentration $[H_2O(0)]$, which is in large excess, is held fixed at its observed atmospheric value, which is shown in Figure 2. The quantities $k_q(E' \rightarrow E)$ are the collisional energy transfer rate constants for the transition $E' \rightarrow E$. The rate constants $j_1(E)$ and $j_2(E)$ are the up-pumping rates constants for photon 1 and photon 2, respectively. These expressions include the solar intensities. In practice, we shall solve the kinetics eqs 9 and 10 using finite sized energy bins. The bins are chosen using the energies of the pure overtones states, i.e

$$\Delta E = E(\nu_{ss},0,0) - E(\nu_{ss} - 1,0,0) \tag{11}$$

We find that only eight bins are required to converge the simulations.

To model the kinetics, we require explicit forms for the rate constants. First, we consider $j_1(E)$, which is the rate constant for the absorption of a solar photon of energy E by ground-state water. The $j_1(E)$ rate constant can be obtained by convoluting experimental absorption cross sections[23] with the solar intensity. Thus

$$j_1(E)\Delta E = \sum_j \sigma_{vib}(0 \rightarrow \nu_j) I(E_j)\Delta E \tag{12}$$

where $\sigma_{vib}(0 \rightarrow \nu_j)$ is the absorption cross section for the transition from the ground vibrational state to ν_j and $I(E)$ is the number of solar photons per unit area, time, and energy. The sum is carried out over all states within each energy bin. The cross sections were calculated by averaging the appropriate lines from the Hitran '96 database[23] over 5 nm intervals. The solar intensities (actinic flux) were obtained at each altitude according to the method proposed in the WMO Report 16,[24] i.e.

$$I_\lambda = I_\lambda^\infty\, T_\lambda^{O_2} \exp(-N_{O_3}\sigma_\lambda^{O_3} - N_{total}\sigma_\lambda^{RS}) \tag{13}$$

Here, I_λ^∞ is the limiting light intensity very high in the atmosphere, and $T_\lambda^{O_2}$ is the transmission of the O_2 column. The ozone column, N_{O_3}, and the total column, N_{total}, are used directly with the ozone absorption cross section, $\sigma_\lambda^{O_3}$ and the Rayleigh scattering cross section, σ_λ^{RS}. These intensities were calculated for a range of altitudes and are shown in Figure 1. The final rate constants, $j_1(E)$, are plotted versus altitude in Figure 4.

The collisional energy transfer rate constants, $k_q(E' \rightarrow E)$, for highly excited water have not been experimentally measured. However, energy relaxation problems have often been successfully modeled using the approximate analytical rate constant in lieu of the exact kinetic rates. Following Troe,[25] therefore, we adopt a simple parametrized approximate form that has often been used previously. We assume that the rate constant can be

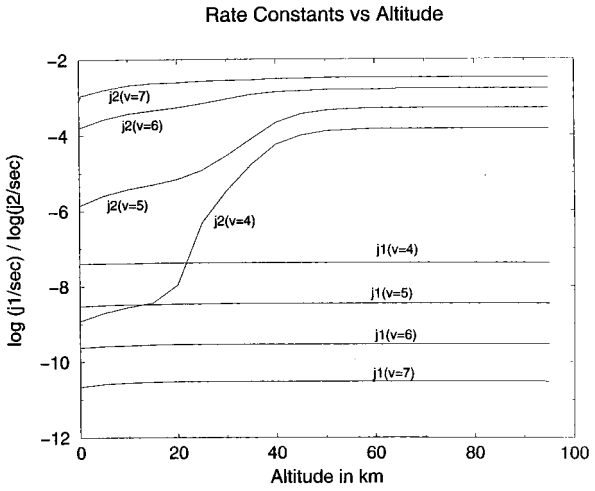

Figure 4. Calculated rate constants vs altitude. The values of computed rate constants, $j_1(E)$ and $j_2(E)$, plotted vs altitude for several values of the symmetric stretch quantum number which labels the energy bins.

composed from the total collision rate constant, Z, and an exponential transition probability, $P(E \rightarrow E')$, i.e.

$$K_q(E \rightarrow E') = ZP(E \rightarrow E') \tag{14}$$

where

$$Z = \sigma\sqrt{\frac{8kT}{\mu\pi}} \tag{15}$$

$$P(E \rightarrow E') = N(E)\begin{matrix} e^{-(E-E')/\alpha} & E > E' \\ e^{-(E'-E)/\beta} & E' > E \end{matrix} \tag{16}$$

The reduced mass, μ, in eq 15 is between that of H_2O and that of the quenching molecule, which we assume to be N_2. The normalization factor $N(E)$ is chosen so that the sum of probabilities to all allowed final states is unity at every energy. The energy bins used in conjunction with eq 16, centered on the asymmetric stretch overtone energies of H_2O^*, are sufficiently widely spaced to ensure that transitions to neighboring energy bins dominate the rates. The requirement of detailed balance relates the values of α and β at a given temperature T

$$\beta = \frac{\alpha}{1 + \alpha/kT} \tag{17}$$

The limiting energy transfer per collision works out to be the monotonic function of α

$$\langle\Delta E\rangle \approx \frac{\Delta E_\uparrow e^{-\Delta E_\uparrow/\beta} - \Delta E_\downarrow e^{-\Delta E_\downarrow/\alpha}}{e^{-\Delta E_\uparrow/\beta} + e^{-\Delta E_\downarrow/\alpha}} < 0 \tag{18}$$

The total collision cross section, σ, is arbitrarily set[26] to the constant value, 10^{-15} cm^2. Thus, the relaxation kinetics is governed by the one parameter, α, which controls the energy transfer efficiency of the collisions.

The rate constant for photodissociation, $j_2(E)$, is the convolution of the absorption cross section for the $\tilde{X} \rightarrow {}^1A_1$ transition with the solar intensity. As with $j_1(E)$, we compute $j_2(E)$ summing over the transitions within each energy bin. Unlike that previous case, however, we must also integrate for all photon energies above the state specific dissociation threshold, i.e.

$$j_2(E)\Delta E = \sum_j \int_{\epsilon_j^{\text{diss}}}^{\infty} \sigma_{\text{dis}}(\nu_j \rightarrow \text{continuum},\epsilon) I(\epsilon)\, d\epsilon \Delta E \tag{19}$$

Here, $\sigma_{\text{dis}}(\nu_j \rightarrow \text{continuum},\epsilon)$ is the photodissociation cross section for the initial state ν_j on the X surface at photon energy ϵ. The solar cutoff will dampen the high-energy parts of the integrand, and thus, the dominant contribution will tend to come from the near-threshold photon energies. The cross sections have not been experimentally measured for vibrationally excited states, so they were computed theoretically. Schinke and co-workers[27] have previously computed absorption spectra for a number of excited states for comparison with the experimental results of Crim and co-workers.[28] Here, we shall carry out similar calculations extended to a broader range of excited states necessary for this process to operate in the atmosphere.

The absorption cross section from an initial eigenstate on the ground surface is given by the standard expression

$$\sigma^{\text{dis}}(E,\nu,J) = \frac{h\nu}{3\pi}|\langle\Psi(E)|\mu_{X,A}|\Phi_{\nu,J}\rangle|^2 \tag{20}$$

In eq 20, Φ represents the ro−vibrational wave function of the initial state on the $\tilde{X}$ surface, Ψ is the final (continuum) nuclear wave function on the upper ${}^1A_1$ surface, and $\mu_{X,A}$ is the transition dipole operator. For a direct dissociation process, it is more efficient to use a time-dependent treatment for the cross section. Hence, we shall compute the cross section from[29]

$$\sigma^{\text{dis}}(E,\nu,J) = \frac{h\nu}{3\pi}\int_{-\infty}^{\infty}\langle\phi_n(0)|\phi_n(t)\rangle e^{i\nu t}\, dt \tag{21}$$

where $\phi_n(t)$ is the solution to the time-dependent Schrödinger equation on the ${}^1A_1$ surface with the boundary condition

$$\phi_n(t=0) = \mu_{X,A}\Phi_n \tag{22}$$

To simplify the computations, we used a reduced dimensionality model to estimate the quantum mechanical quantities. Specifically, we assume a two-dimensional representation of the nuclear motion that includes the two stretching models of H_2O at the equilibrium bond angle $\theta = 104.5°$but not the bending or rotational modes. The bending zero-point energy is included. Effectively, this assumes that the dissociation process (which is an asymmetric stretch motion) is fast compared to either the rotation or the bending motion. The wave packet propagation was carried out using a method described in detail elsewhere.[30]

As input into the quantum dynamics calculations, we require explicit forms for the Born−Oppenheimer potential surfaces of the $\tilde{X}$ and ${}^1A_1$ states and for the transition dipole function $\mu_{X,A}$. For the $\tilde{X}$ state surface, we employed the potential of Tennyson and co-workers.[31] This potential was found to be consistent with the experimental spectrum of the H_2O molecule and should be adequate for our purposes. The upper-state ${}^1A_1$ potential was taken to be the expression of Schinke and co-workers,[27] which was based on a fitting of ab initio calculations. Consistent with the Schinke potential, we chose the dipole function present in ref 27. We employ the smoothing technique of Zhang et al.[32] to extend the function beyond the original domain used for the fitting.

Obviously, our model makes significant approximations to the true photodissociation dynamics. In addition to neglecting the bending and rotational motion during the dissociation process, we do not enforce the nuclear and electronic angular momentum constraints. However, since we are only interested in obtaining an estimate of the total cross section for a kinetic

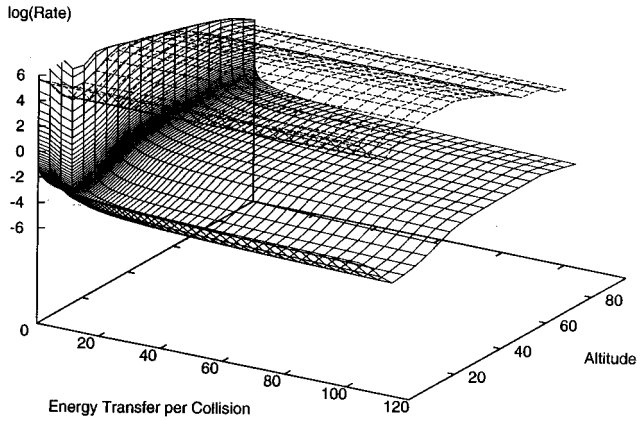

Figure 5. Production rate of HO_x, molecules/cm^{3}sec, vs collision efficiency in cm^{-1}/collision and altitude in km. The two-photon mechanism shows a dramatic dependence on collision efficiency at low values. Also plotted is the prediction of standard mechanism, eqs 1−4, which does not depend on the collision efficiency.

analysis of OH production and not in detailed state-to-state dynamics, we believe that this treatment is adequate. To compensate for the approximation, we introduce a normalization factor to make the computed cross section agree with known experimental results. The experimental and theoretical cross section for the $\tilde{X}(0,0,0) \rightarrow {}^1A_1$ band is integrated over frequency to obtain the factor

$$N = \frac{\int \sigma_{\text{exp}}(\nu)\, d\nu}{\int \sigma_{\text{theor}}(\nu)\, d\nu} \tag{23}$$

that is then multiplied by the theoretical prediction. The value of N is close to 1. Of the approximations made, the neglect of the bending motion is probably the most significant. As a test of the two-dimension model, we have carried out a three-dimensional simulation of the photodissociation for comparison. The agreement between the cross sections is reasonably good, within about 25%, when the bend zero point is included. The rate constants, $j_2(E)$, obtained from this calculation are plotted in Figure 4.

IV. Results and Discussion

The kinetic eqs 9 and 10 were simulated using a standard stiff differential equation solver (LSODE)[33] as a function of the altitude and the energy relaxation parameter, α. The kinetic production rate of HO_x was extracted from the steady-state solutions to the differential equations, i.e., the long time asymptotic behavior. For all but the smallest values of α, the steady state was approached quite rapidly, $\ll$1 s. In Figure 5, the resulting production rates are plotted on a logarithmic scale versus altitude and the energy transfer per collision. The profound effect of the collision efficiency on the overall mechanism is apparent from the figure. At low collision efficiency, the rate is dominated by the vibrational up-pumping process, eq 7. Indeed, it is clear from eqs 9 and 10 that in the limit of $\alpha \rightarrow 0$, the $j_1(E)$ rate constants become rate governing. There is a rapid fall off in the HO_x rate as α is increased. At high collision efficiency, for all altitudes, the production rate flattens out at very low values, $\sim 10^{-4}-10^{-5}$ mol/cm^3 sec.

Also plotted in Figure 5 is the HO_x production rate predicted by the conventional mechanism. Of interest here is when the two-photon mechanism becomes competitive with the conventional mechanism. At high collision efficiency, it is clear that the conventional mechanism dominates. At high (stratospheric) altitudes and low (tropospheric) altitudes, the two-photon photodissociation becomes commensurate to eqs 1−4 for small values of the collision efficiency. The intersection of the two surfaces in Figure 5 forms a curve as a function of altitude, which gives the value of α required for the two mechanisms to yield equal rates. It is clear that collision efficiency must be quite low, less than 1 cm^{-1} per collision, for the two-photon mechanism to become competitive. The observed error for OH production in the standard model is on the order of several percent. Thus, at 50 km, the collision efficiency would have to be 0.15 cm^{-1}/collision for the two-photon mechanism to give a 3% correction to the prediction of the standard model.

As mentioned above, the actual vibrational relaxation rates for highly excited water have yet to be measured in the laboratory. However, we suspect that the rates required for the two-photon mechanism to be significant may be much lower than the true values. On the basis of the observed relaxation rates of other highly excited triatomic molecules such as SO_2 and CS_2, a value of 50 cm^{-1}/collision seems typical. Hovis and Moore[34] have obtained the relaxation rate of $H^{18}{}_2O$ with N_2 from a low-lying vibrational state. The value of obtained, $\sim$ 8 cm^{-1}/collision, is too large for a significant contribution from the two photon mechanism. Although relaxation from higher energy vibrational states may significantly differ from this result, it would be unusual if the rate were an order of magnitude lower.

We should note that solar pumping of vibrational overtones of atmospheric chromophores containing OH, such as HNO_3, HNO_4, and H_2O_2, has recently been proposed[11] to account for the high zenith angle discrepancy between the [OH] by Wennberg et al.[35] and the standard model results. This mechanism, in contrast with the one proposed here, involves one-photon dissociation on the ground potential energy surface and makes little contribution as a new OH source at low zenith angle. Under these conditions, sufficient ultraviolet radiation exists to pump directly the dissociative electronic states of the chromophores. The electronic states of water, however, can be accessed only at wavelengths shorter than 185 nm, and the water bond dissociation energies are too high to be accessible by solar photons. Consequently, the vibrational overtone mediated sequential two-photon process proposed here could in principle play a role in OH production from water photolysis in the atmosphere.

V. Conclusions

We propose a two-photon mechanism for photolysis of water vapor and investigate the rate of atmospheric hydroxyl radical formation by solar pumping. The rate of OH formation depends nonlinearly on the collision efficiency for vibrational energy transfer from H_2O^* with N_2 and O_2 and can be significant only at very low collision efficiencies. The kinetic model developed in this paper gives a general form for the rate of OH production, which can be compared with the rate of OH formation by the standard mechanism of $O(^1D)$ reaction with H_2O and CH_4. Both mechanisms depend on the concentration of H_2O, which decreases rapidly with increasing altitude. The standard mechanism relies on O_3 photolysis to produce $O(^1D)$ and is most efficient in the lower stratosphere. By comparison, the proposed two-photon mechanism is expected to become relatively more significant at low altitude in the troposphere and also at high altitude in the upper stratosphere above the ozone layer.

Atmospheric measurements of OH have improved significantly and are able to observe small discrepancies (<10%) between measured OH concentrations and the predictions of

atmospheric models. At most altitudes where data is available, models underestimate atmospheric OH concentrations. Consistent with the small discrepancies between current models and measurements, we expect that the proposed vibrationally mediated mechanism will be a minor, yet conceptually interesting, contribution to hydroxyl radical formation in the atmosphere. The results presented here depend critically on the rate of collisional energy transfer out of the high vibrational levels of H_2O. While it appears unlikely that the vibrational quenching efficiency will turn out to be low enough for the two photon mechanism to contribute significantly, a final conclusion of course must await experimental measurement of this quantity.

Acknowledgment. This work was supported by Grant NSF-9725549 from the National Science Foundation. We are grateful to Reinhardt Schinke for providing the excited-state potential surface and to Jonathan Tennyson for providing the ground-state potential function.

References and Notes

(1) Wayne, R. P. *Chemistry of Atmospheres*, 2nd ed.; Clarendon Press: Oxford, 1991.

(2) Brasseur, G.: Solomon, S. *Aeronomy of the Middle Atmosphere*, 2nd ed.;Reidel: Dortrecht, The Netherlands, 1986.

(3) Finlayson-Pitts, B. J.; Pitts, J. N. *Atmospheric Chemistry: Fundamentals and Experimental Techniques*; Wiley: New York, 1986.

(4) *World Meteorological Organization Global Ozone Research and Monitoring Project*; Report No. 44; NASA: Washington, DC1999.

(5) Ball, S. M.; Hancock, G.; Martin, S. E.; Pinot de Moira, J. C. *Chem. Phys. Lett.* **1997**, *264*, 531.

(6) Brewer, A. H. *Q. J. R. Meteorol. Soc.* **1949**, *75*, 351.

(7) Wang, H. T.; Felps, W. S.; McGlynn, S. P. *J. Chem. Phys.* **1977**, *67*, 2614.

(8) Hampson, J. *Les Problemes Meteorologigue de la Stratosphere et de la Mesosphere*; Presses Universitaires de France: Paris, 1965.

(9) Levy, H. *Science* **1971**, *173*, 141.

(10) Salawitch, R. J.; et al. *Geophys. Res. Lett.* **1994**, *21*, 2551. Hanson, D. R.; Ravishankara, A. R. *Geophys. Res. Lett.* **1995**, *22*, 385.

(11) Donaldson, D. J.; Frost, G. J.; Rosenlof, K. H.; Tuck, A. F.; Vaida, V. *J. Geophys. Res.* **1997**, *24*, 2651.

(12) Frost, G. J.; Vaida, V. *J. Geophys. Res.* **1995**, *100*, 18803.

(13) Muller, R.; Salawitch, R. J. In *World Meteorological Organization Global Ozone Research and Monitoring Project*; Report No. 44; NASA: Washington, DC 1999; Chapter 6.

(14) Ravishankara, A. R.; Shepherd, T. G. In *World Meteorological Organization Global Ozone Research and Monitoring Project*; Report No. 44; NASA: Washington, DC, 1999; Chapter 7.

(15) Wennberg, P. O.; et al. *Science* **1994**, *266*, 398. Wennberg, P. O.; et al. *J. Atmos. Sci.* **1995**, *52*, 3413.

(16) Mauldin, R. L., III; Mandronich, S.; Flocke, S. J.; Eisle, F. L.; Frost, G. J.; Prevot, A. S. H. *Geophys. Res. Lett.* **1997**, *24*, 3033.

(17) Frost, G. J.; Trainer, M.; Mauldin, R. L., III; Eisle, F. L.; Prevot, A. S. H.; Flocke, S. J.; Mandronich, S.; Kok, G.; Schillowski, R. D.; Boumgardner, D.; Bradshaw, J. *J. Geophys. Res.* **1999**, *104*, 16041.

(18) Mount G. H.; Williams, E. J. *J. Geophys. Res.* **1997**, *10*, 6171.

(19) Comes, F. J.; Forberich, O.; Walter, J. *J. Atmos. Sci.* **1997**, *54*, 1886.

(20) Doherty, G. M.; Newell, R. E. *Tellus* **1984**, *36B*, 149. Ludlam, F. H. *Clouds and Storms*; Pennsylvania State University Press: University Park, PA, 1980. V. Ramanathan, V.; Vogelmann, A. M. *Ambio* **1997**, *26*, 38. Tyndall, J. *Philos. Trans. R. Soc.* **1861**, *A151*, 1.

(21) Rothman, L. S.; Rinsland, C. P.; Goldman, A.; Massie, S. T. *J. Quant. Spectrosc. Radiat. Transfer* **1998**, *60*, 665.

(22) Barnes, P. W.; Sharkey, P.; Sims, I. R.; Smith, I. W. M. *J. Chem. Soc., Faraday Discus.* **1999**, *113*, 167.

(23) Rothman, L. S.; et al. *J. Quant. Spectrosc. Radiat. Transfer* **1992**, *48*, 469.

(24) *World Meteorological Organization, Global Ozone Research and Monitoring Project: No. 16*; NASA, Washington, DC, 1985.

(25) Troe, J. *J. Chem. Phys.* **1977**, *66*, 4745.

(26) Since we shall consider the kinetics over a continuous range of α values, the exact value chosen for σ is not crucial. The important quantity is the overall energy transfer rate, which is governed by rate constants.

(27) Engel, V.; Schinke, R.; Staemmler, V. *J. Chem. Phys.* **1987**, *88*, 129. Van der Wal, R. L.; Scott, J. L.; Crim, F. F.; Weide, K.; Schinke, R. *J. Chem. Phys*. **1991**, *94*, 3548.

(28) Van der Wal, R. L.; Scott, J. L.; Crim, F. F. *J. Chem. Phys*. **1991**, *94*, 1859. Van der Wal, R. L.; Scott, J. L.; Crim, F. F. *J. Phys. Chem*. **1989**, *93*, 5331. Crim, F. F. *Annu. Rev. Phys. Chem*. **1993**, *44*, 397. Crim, F. F. *J. Phys. Chem*. **1996**, *100*, 12725.

(29) Heller, E. J. *J. Chem. Phys*. **1978**, *68*, 3891.

(30) Sadeghi, R.; Skodje, R. T. *J. Chem. Phys*. **1993**, *98*, 9208; **1996**, *105*, 7504. Skodje, R. T.; Sadeghi, R.; Krause, J. R.; Koppel, H. *J. Chem. Phys.* **1994**, *101*, 1725.

(31) Polyonsky, O. L.; Jensen, P.; Tennyson, J. *J. Chem. Phys.* **1996**, *105*, 6490.

(32) Zhang, J.; Imre, D. G. *J. Chem. Phys.* **1989**, *90*, 1666.

(33) Hindmarsh, A. C. *ACM SIGNUM Newslett.* **1980**, *15*, 10.

(34) Hovis, F. E.; Moore, C. B. *J. Chem Phys.* **1980**, *72*, 2397.

(35) Wennberg, P. O.; et al. *Geophys. Res. Lett.* **1999**, *26*, 1373.